FEATURE ARTICLE

Symmetry-Controlled Colloidal Nanocrystals: Nonhydrolytic Chemical Synthesis and Shape Determining Parameters

Young-wook Jun, Jae-Hyun Lee, Jin-sil Choi, and Jinwoo Cheon*

Department of Chemistry and Nano-Medical National Core Research Center (NCRC), Yonsei University, Seoul 120-749, Korea

Received: May 1, 2005; In Final Form: June 1, 2005

Since inorganic nanocrystals exhibit unique shape-dependent nanoscale properties and can be utilized as basic building blocks for futuristic nanodevices, a systematic study on the shape control of these nanocrystals remains an important subject in materials and physical chemistry. In this feature article, we overview the recent progress on the synthetic development of symmetry-controlled colloidal nanocrystals of semiconductor and metal oxide, which are prepared through nonhydrolytic chemical routes. We describe their shape-guiding processes and illustrate the detailed key factors controlling their growth by examining various case studies of zero-dimensional spheres and cubes, one-dimensional rods, and quasi multidimensional structures such as disks, multipods, and stars. Specifically, the crystalline phase of nucleating seeds, surface energy, kinetic vs thermodynamic growth, and selective adhesion processes of capping ligands are found to be most crucial for the determination of the nanocrystal shape.

I. Introduction

In a nanoscale regime, chemical and physical properties of inorganic crystals are highly dependent on geometrical factors such as size and shape.[1−3] Precise control of such factors allows one not only to observe unique properties of the nanocrystals but also to tune their chemical and physical properties as desired. During the past decades, researchers have been exploring efficient synthetic routes of well-defined inorganic nanocrystals with a controlled size and shape. Gas-phase syntheses such as the vapor−liquid−solid (VLS) method and thermal evaporation are powerful tools for the controlled fabrication of nanocrystals.[4−12] Some advanced nanocrystal structures with interesting geometries including wires,[4−6] tubes,[7,8] ribbons,[9] and more complex shapes[10−12] are good examples of successful utilization of the gas-phase approaches. On the other hand, the colloidal approach in liquid media provides convenient and reproducible routes for the fabrication of nanocrystals with a controlled size and shape.[13−51] This enables the resulting nanocrystals not only to be precisely tuned at the sub-10 nm scale but also to be easily dispersed in organic or aqueous media for the numerous potential applications in electronics and biological systems. For example, the size of CdSe nanospheres can be tuned from ∼1 to 12 nm with one nanometer resolution by controlling growth parameters, and the resulting nanocrystals are soluble either in typical organic or aqueous media by controlling the surface capping molecules.[13] Along with such size controllability, anisotropic shape controllability of nanocrystals has been attained through liquid methods.[14−51]

The nonhydrolytic molecular precursor decomposition method is an effective route for the controlled synthesis of both isotropic and anisotropic colloidal nanocrystals.[19] Typically molecular precursors are injected into a hot (∼100−350 °C) organic solvent containing capping molecules, which induces (i) a rapid increase of the monomer concentration, (ii) nanocrystal growth through aggregation of the monomers, and (iii) surface passivations of the resulting nanocrystals with capping molecules. Nanocrystals obtained by such nonhydrolytic synthetic methods in general possess excellent crystallinity and monodispersity in terms of size and shape. Moreover, this method has several controllable synthetic aspects: (i) facile separation between nucleation and growth stages, (ii) control of growth parameters such as the choice of the molecular precursor and capping molecules, the reaction temperature, and the growth time. Such advantages have enabled successful syntheses of a wide range of high quality nanocrystals including semiconductors,[20−34] transition metal oxides[35−43] and sulfides,[44,45] metals,[46−50] and lanthanide metal oxides.[51] Although there are increasing numbers of examples of colloidal nanocrystals with anisotropic shapes, from simple one-dimensional rods and wires to advanced multipods and stars, reports on their shape-guiding mechanism are very limited. To obtain more advanced-structured nanocrystals and to have the ability to control the nanocrystal shape as desired, the unraveling and systematic understanding of shape-guiding processes is necessary.

In this feature article, we present an overview and recent progress in the development of colloidal nanocrystals with various symmetry-controlled shapes. We focus on the semiconductor and metal oxide nanocrystals synthesized through the nonhydrolytic chemical route, with particular emphasis on the current understanding and achievement of nanocrystal shape controls. Critical parameters for the nanocrystal shape determination are discussed through the case studies of nanocrystal

* Corresponding author: jcheon@yonsei.ac.kr.

10.1021/jp052257v CCC: $30.25
Published on Web 08/04/2005

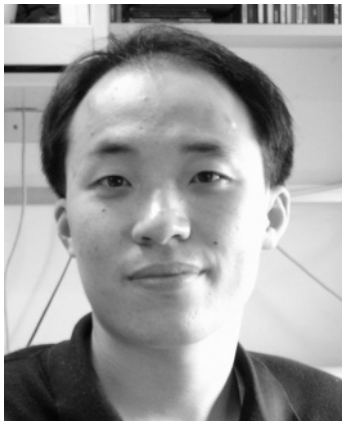

Young-wook Jun earned his B.S. degree in chemistry from Yonsei University (1999) and his Ph. D. degree in chemistry from the Korea Advanced Institute of Science and Technology (KAIST) (2005), where he studied the controlled synthesis and assembly of colloidal inorganic nanocrystals under the guidance of Professor Sang Youl Kim and Professor Jinwoo Cheon. Currently, he is carrying out postdoctoral studies as a member of Professor Cheon's group at Yonsei University. He is a recipient of the Honorable Mention Award of the IUPAC Prize for Young Chemists (2005). His current research focuses on the development of smart inorganic nanocrystal−biomolecule hybrid systems for biomedical imaging and sensor applications.

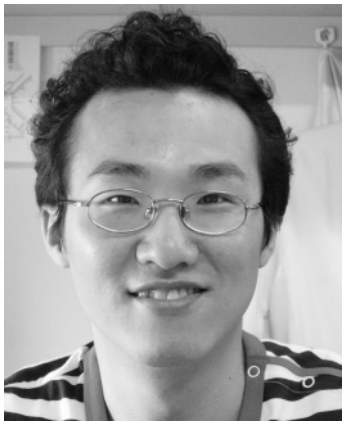

Jae-Hyun Lee was born in Seoul, Korea and graduated from Yonsei University in 2003 with his B.S. degree in chemistry. Currently, he is a third year graduate student in his Ph.D. program under the supervision of Professor Jinwoo Cheon. He is a winner of a Korea Research Foundation fellowship for superior ability graduate student (2004). His research interests include the synthesis of inorganic nanocrystals and the development of multifunctional biocompatible nanocrystals for biomedical applications.

growths of various semiconductors (e.g., CdS, MnS, $Cd_{1-x}Mn_xS$, GaP, PbS) and transition metal oxides (e.g., TiO_2, $W_{18}O_{49}$, Mn_3O_4).

II. General Symmetrical Motifs of Inorganic Nanocrystals

Inorganic nanocrystals can be classified according to dimensionality and crystal symmetry (Figure 1). Highly symmetric isotropic spheres, cubes (symmetry group: O_h), tetradecahedrons (O_h), and tetrahedrons (T_d) can be classified as zero-dimensional nanostrucutures. Various spherical shapes of semiconductors, metal oxide, and metal nanocrystals have been synthesized through nonhydrolytic chemical methods. Rods, wires, and pipes ($D_{\infty h}$) are examples of one-dimensional strucutures. Since CdSe nanorods were first reported by Alivisatos and co-workers,[19] studies on the synthesis of one-dimensional nanostructures have been extensively carried out. Included in this group are rods and wires of group II−VI semiconductors (e.g., CdS,[20−22] CdSe,[19,20,23,24] CdTe,[20,25,26] ZnSe[27]), III−V semiconductors (GaP,[28] InP[29]), IV semiconductor (Ge[30]), other semiconductors (PbS,[31] PbSe,[32,33] MnS[21,34]), and transition metal oxides (e.g., ZnO,[35,36] TiO_2,[37−39] $W_{18}O_{49}$,[39,40] Mn_3O_4,[39,41] V_2O_5,[37] $BaTiO_4$,[42] and Fe_3O_4[43]). These one-dimensional nanostructures exhibit novel optical and magnetic properties arising from shape anisotropy. Disks ($D_{\infty h}$) and plates with polygon shapes (D_{nh}) belong to quasi two-dimensional nano building blocks. Quasi two-dimensional transition metal sulfide, Cu_2S[44] and NiS[45]

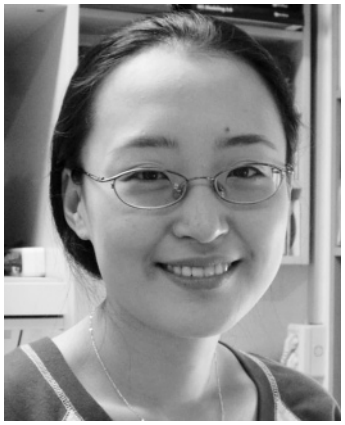

Jin-sil Choi was born in 1980 in Daegu, Korea. She received her B.S. degree in chemistry from Yonsei University in 2004 and now is a second year graduate student pursuing her Ph.D. degree at Yonsei University under the supervision of Prof. Jinwoo Cheon. Her current research interests are the fabrication of shape-, size-, and composition-controlled multicomponent inorganic nanocrystals and their biocompatibility and safety evaluation on biological systems.

Jinwoo Cheon is a Professor of Chemistry at Yonsei University and Head of the Nanomaterials Division of the Nano-Medical National Core Research Center of Korea. He received his B.S. and M.S. degrees in chemistry from Yonsei University in Seoul, Korea. He then moved to the University of Illinois, Urbana-Champaign where he earned his Ph.D. in organometallics and materials chemistry from Prof. G. Girolami in 1993. After receiving post-doctoral training at the University of California, Berkeley, with Prof. J. Arnold and Dr. E. Bourret in the field of molecular precursor chemistry for semiconducting materials and also at UCLA with Prof. J. Zink studying the photochemistry of inorganic materials, he joined the Korea Advanced Institute of Science and Technology (KAIST) as an assistant professor in 1998. In 2002, he moved to Yonsei University where he was appointed full professor of chemistry. Professor Cheon was elected as a junior member of the Korean Academy of Science and Technology in 2003 and is a recipient of the Korean Chemical Society Award in Inorganic Chemistry (2004), the National Science Prize for Junior Faculty (2002), and the Korean Chemical Society−Wiley Young Chemist Award (2001). His research areas include the fabrication and shape control of inorganic nanocrystals, hierarchical self-assembly, nanoscale biomagnetics, and the applications of nanocrystals for biomedical sciences such as targeting, trafficking, and imaging of biomolecules via optical and magnetic resonance imaging techniques.

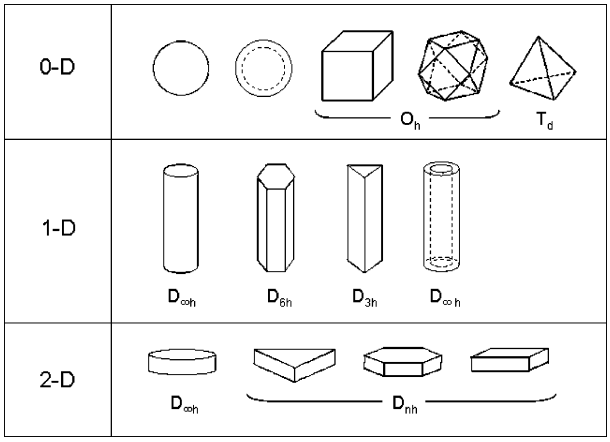

Figure 1. Various symmetrical motifs of inorganic nanocrystals.

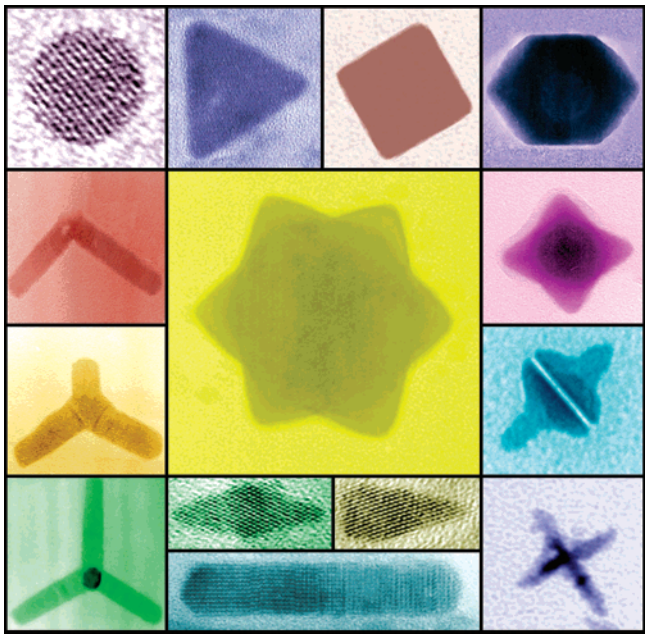

Figure 2. Galleries of chemically synthesized inorganic nanocrystals with various shapes.

nanodisks ($D_{\infty}h$), Co metal nanodisks ($D_{\infty h}$),[46,47] Gd_2O_3 nanodisks ($D_{\infty h}$),[51] and Fe_2O_3 trigonal prisms (D_{3h})[43] have been recently reported, but there is no report on two-dimensional semiconductor nanocrystals by nonhydrolytic chemical routes.

In addition to such primative shapes of inorganic nanocrystals, advanced shapes of nanocrystals have been developed. Multipod structures of semiconductors (e.g., CdS,[20] CdSe,[23] CdTe,[25] MnS,[34] ZnSe[27]) including bipods (C_{2v}), tripods (C_{3v}), and tetrapods (T_d), star-shaped PbS (O_h) nanocrystals,[31] and dedritic CdSe[23] and CdTe[25] nanocrystals are examples of such cases.

Representative symmetry-controlled nanocrystalline shapes synthesized by nonhydrolytic chemical routes are displayed in Figure 2. In the following sections, we will discuss the synthesis of these nanocrystals and the critical parameters for the shape determinations.

III. Critical Parameters for the Nanocrystal Shape Determination

Nanocrystal formation can be simply understood as two-step processes: (i) nucleation initiated by sudden increase of monomer concentration up to super-saturation levels, and (ii) the subsequent growth from the seed with progressive consumption of monomers in solution (Figure 3). The final geometry of

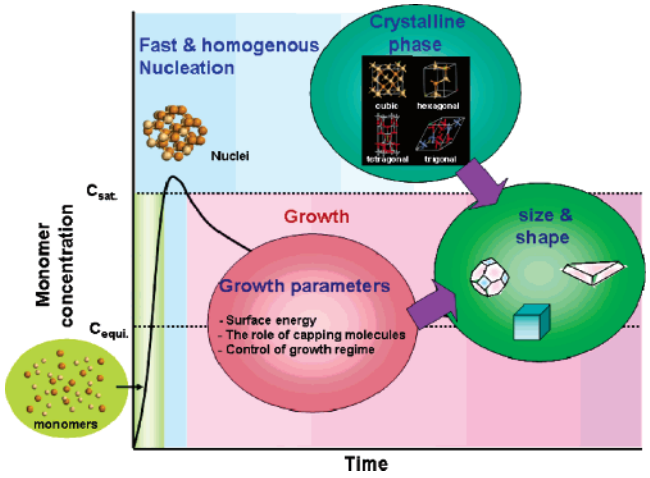

Figure 3. Crystal growth processes and key factors for shape determination.

nanocrystals is determined by several parameters during these nucleation and growth processes. Initially, the crystalline phase of the seed at the nucleating stage is the critical parameter for directing nanocrystal shapes due to its characteristic unit cell structure. Once nanocrystal seeds are formed with a specific crystalline phase, several other factors for controlling the subsequent growth processes will affect the final geometry of nanocrystals. Such key factors include the intrinsic surface energy of different crystallographic surfaces, the role of surface selective capping molecules, and the choice of the nanocrystal growth regime between thermodynamic and kinetic processes.

We describe the effect of key factors on the nanocrystal shape determination, including (i) crystalline phase effect of seeds, (ii) surface energy effect, and (iii) control of the growth regime. By changing reaction parameters, systematic manipulation of these key parameters is possible, which finally yields various symmetry-controlled nanocrystals.

a. Crystalline Phase Effect of Nucleating Seeds on the Final Nanocrystal Geometry. Nucleating seeds of nanocrystals can potentially have a variety of crystalline phases from isotropic structure of cubic to anisotropic structure of hexagonal or monoclinic. Among various crystalline phases, the stable phase of materials is highly dependent on its environment such as temperature and the choice of capping molecules. For example, by adjusting the initial temperature during the nucleation process, the crystalline phase of nanocrystals can be controlled. Once the crystalline phase is determined, the characteristic unit cell structures of the seeds strongly affect on the further nanocrystal growth process. For example, an isotropic unit cell structure (e.g., cubic) of the seed generally induces the isotropic growth of nanocrystals from the seed, and therefore zero-dimensional nanostructures are expected. In contrast, anisotropic unit cell structures of the seed can induce anisotropic growth along crystallographically reactive directions, and therefore anisotropic shapes of nanocrystals are expected. The growth of MnS nanocrystals can be a good example.[34] MnS crystals possess diverse crystallographic structures from isotropic rock-salt structure and zinc blende to anisotropic wurtzite. It is known that the rock-salt structure is more stable at high temperature (>200 °C), whereas the wurtzite structure is preferred at temperatures below 200 °C.[52,53] At high temperature (~200 °C), the seeds of rock-salt structured MnS induces isotropic growth along eight {111} directions, and 30-nm sized nanocubes are easily observed after the injection of the molecular precursor, $Mn(S_2CNEt_2)_2$, into hot hexadecylamine capping molecules

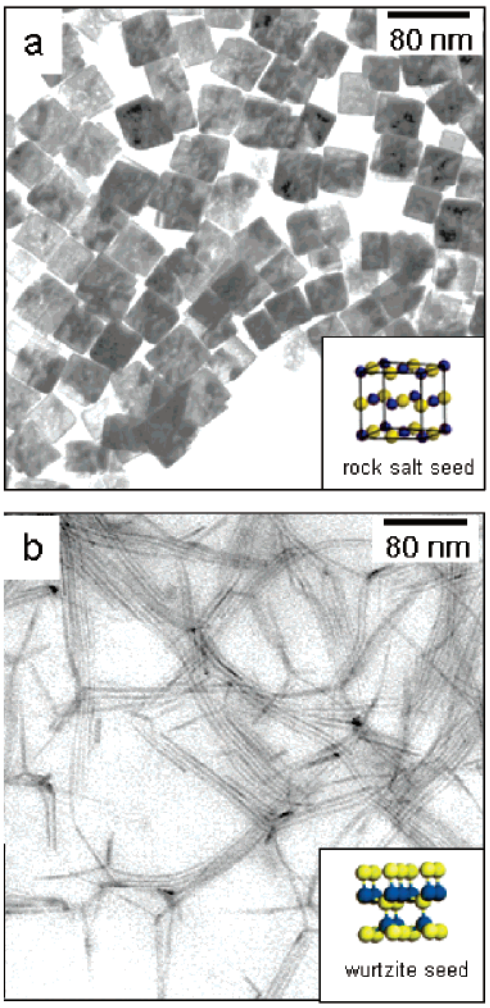

Figure 4. Crystalline phase effects on shape determination of MnS nanocrystals. (a) nanocubes obtained at ~200 °C, (b) nanowires obtained at ~120 °C.

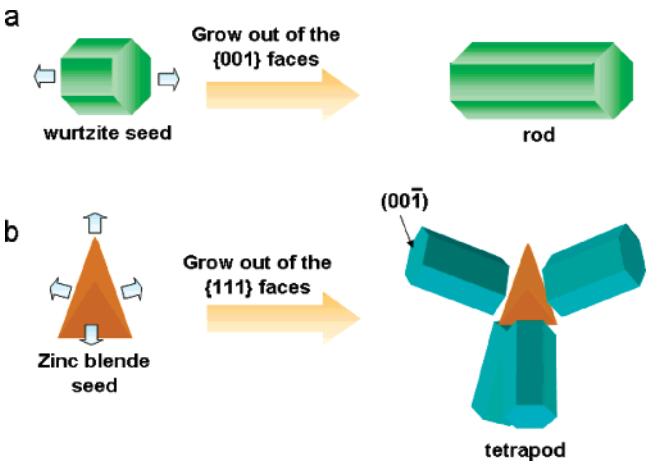

Figure 5. CdS nanocrystal growth: (a) monorods from hexagonal wurtzite seeds, (b) tetrapods from zinc blende seeds.

(Figure 4a). In contrast, at low temperature (~120 °C), the nucleation with the hexagonal wurtzite structure results in anisotropic growth along the *c*-axis of wurtzite structures and therefore very thin nanowires of 2 nm in diameter with an aspect ratio of ~80 are obtained (Figure 4b).

Similar crystalline phase effects of the seeds can be observed in the case of CdS nanocrystal growth.[22] CdS has two distinct crystalline phases: an isotropic zinc blende is stable below 250

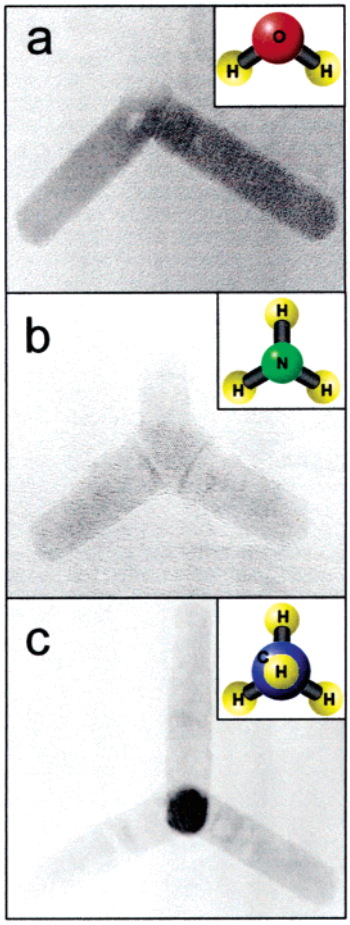

Figure 6. Various multipod shapes of CdS: (a) bipod, (b) tripod, (c) tetrapod.

°C and hexagonal wurtzite is preferred at high temperature (~300 °C).[54] At high temperature, exclusive formation of one-dimensional CdS rods is observed from high temperature stable wurtzite structured seeds, as similarly seen in the MnS nanowire growth (Figure 5a). However, at lower temperatures, the formation of tetrahedral shapes of zinc blende seeds truncated with four {111} faces is facilitated.[54] The subsequent epitaxial growth of wurtzite pods along the *c*-axis from the four equivalent {111} faces of the seed results in the formation of CdS tetrapods (Figure 5b, 6c). In addition, through fine-tunings of the growth temperature and monomer concentration, low valent shapes of multipods such as monorods, bipods, and tripods from the zinc blende seeds can be obtained (Figure 6). High resolution transmission electron microscopic (HR-TEM) analyses clearly show the crystalline phase effect of the CdS monorod and multipod growth. The monorods prepared at high temperature have hexagonal wurtzite structures (Figure 7a). In contrast, the HR-TEM image of bipods prepared at lower temperatures indicates that the the core is of cubic zinc blende structure with tetrahedral geometry and a separation angle of ~109.5° between arms of the bipods (Figure 7b). Similarly, pencil-shaped monorods synthesized at low temperature (~120 °C) have the zinc blende structured seed at the one end of the rod (Figure 7c).

In addition to such temperature-mediated crystalline phase control of seeds, the choice of capping molecules can be a means of controlling the crystalline phase of seeds. Since the capping molecules dynamically bind to the crystal surface during the nucleation and crystal growth, the conformation of crystal structure is highly affected by the identity of the capping

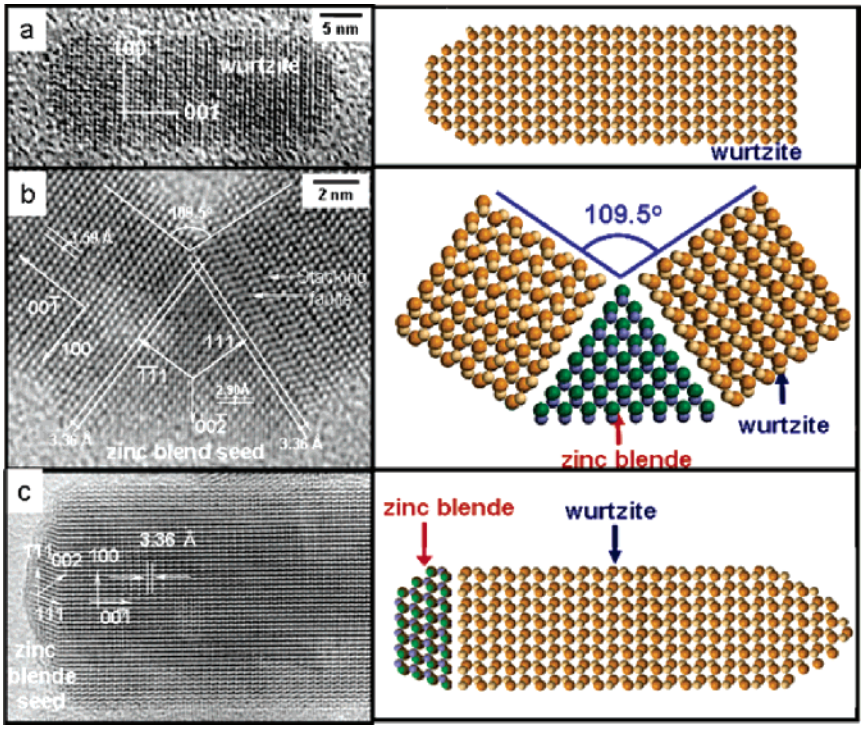

Figure 7. HR-TEM analyses of CdS nanocrystals: (a) monorod at 300 °C, (b) bipods at 180 °C, (c) pencil-shaped rod at 120 °C.

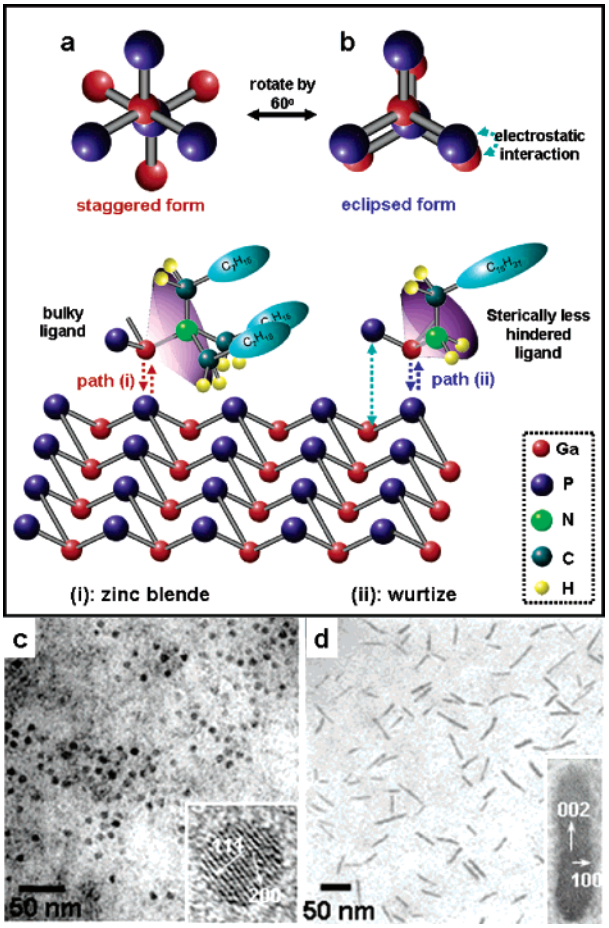

Figure 8. Capping molecule mediated seed formation of GaP nanocrystals: (a) staggered conformation of the zinc blende structures, (b) eclipsed structures of the wurtzite structure, (c) zinc blende structured GaP nanospheres, (d) wurtzite structured GaP nanorods. Path (i) sterically favored seed formation under the use of trioctylamine, path (ii) electronically favored seed formation under the use of hexadecylamine.

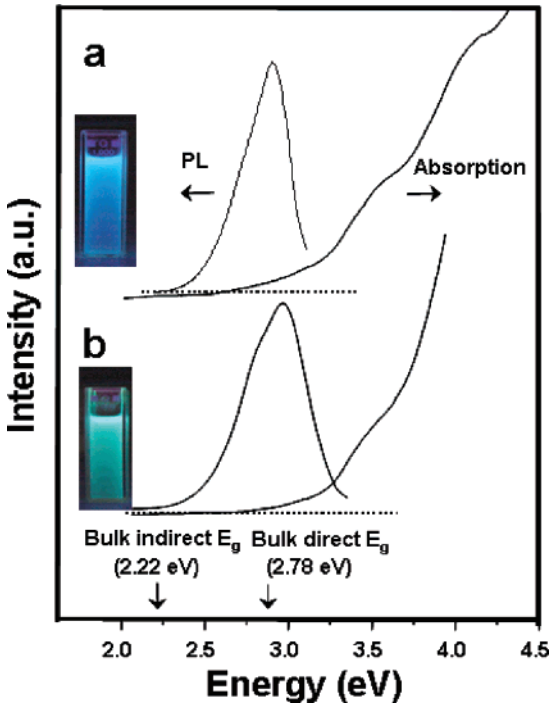

Figure 9. Anistropic effect on the optical properties of GaP nanocrystals. UV−vis absorption and photoluminescence spectra of (a) GaP nanospheres and (b) GaP nanorods.

molecules. GaP have two distinct crystalline phases that are in rotational isomerism: the zinc blende phase, which is a staggered conformation with ⟨111⟩ directions, and the wurtzite phase, which is an eclipsed conformation with ⟨001⟩ directions (Figure 8a,b). Zinc blende GaP is a thermodynamically stable phase that is sterically favored.[55] Wurtzite GaP is a kinetically stable phase that is favored due to the electrostatic interaction between geminal gallium and phosphine atoms when GaP monomers approach the crystal surface.[55] The energy difference between these two phases is subtle, and control of the steric

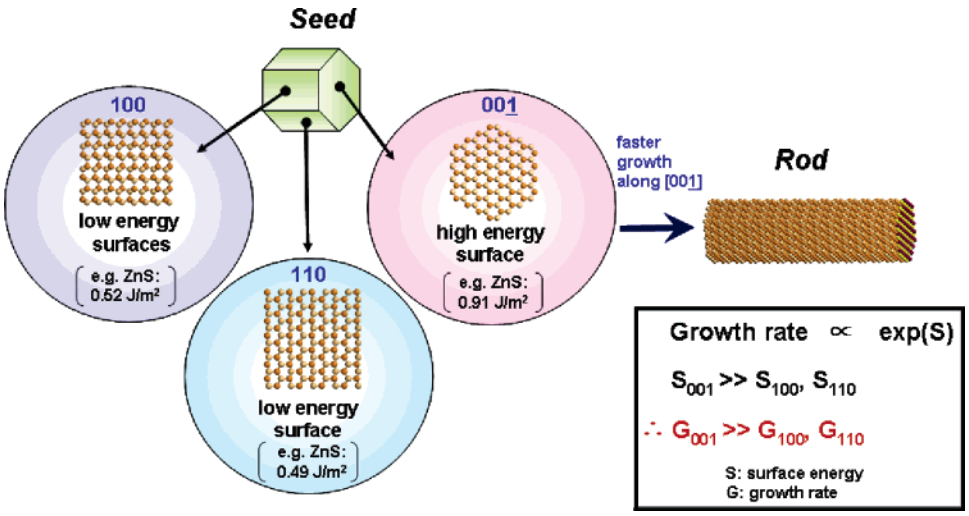

Figure 10. Surface energy initiated anisotropic growth of one-dimensional semiconductor nanorods with wurtzite structures.

effect of GaP monomer molecules can have a significant affect on the conformation of crystal structures.[28] When sterically bulky tertiary amines (e.g., trioctylamine) are used as capping molecules, the staggered conformation is highly favored due to the large steric hindrance between tertiary amine capping molecules and the crystal surface. (Figure 8, path (i)) Therefore, formation of zinc blende GaP nanospheres results (Figure 8c). However, when sterically less hindered primary amines (e.g., hexadecylamine) are used, the steric energy difference between eclipsed and staggered conformations is diminished. Therefore, steric effects on determining the binding geometry of incoming monomers are now minor and electronic effects play a major role. This facilitates the formation of the kinetically stable wurtzite GaP (Figure 8, path (ii)) and further induces the formation of rod-shaped nanocrystals elongated along the *c*-axis under the kinetic growth regime induced by a high monomer concentration (Figure 8d). The GaP nanocrystals obtained exhibit unique shape-dependent optical features originating from quantum mechanical effects (Figure 9). The absorption spectra show strong shoulders (3.48 and 3.46 eV for spheres and rods, respectively) and shallow tails that are attributed to direct and indirect transition, respectively.[56] The photoluminescence maximum is 2.94 eV for spheres corresponding to the direct transition of 8 nm GaP, while red shift (2.79 eV) is observed for rods (8 × 45 nm), which may arise from shape anisotropy.[57]

b. Surface Energy Effect: Intrinsic Crystallographic Surface Energies and Their Modulation by the Use of Surface Selective Capping Molecules. After the crystalline phase of nucleating seeds is determined, several parameters during the subsequent growth stages strongly govern the final shapes of nanocrystals. One of the critical parameters influencing the growth patterns of nanocrystals is the surface energy of the crystallographic faces of the seed. Since the crystal growth rate is closely related to the nanocrystal surface energy, it is important to examine the surface energy related effects on the anisotropic growth of nanocrystals.

The anisotropic rod growth of hexagonal wurtzite semiconductors demonstrated by us (CdS, MnS, and GaP) and by others (e.g., CdSe,[19,20,23,24] CdTe,[25] ZnSe[27]) is driven by this surface energy effect. In general, the surface energy of {001} faces of the wurtzite structure is much larger than those of other faces such as {100} and {110} due to the high packing density and a large number of under-coordinated atoms of the {001} faces (Figure 10). Such surface energy difference results in significant growth rate differences between different crystallographic

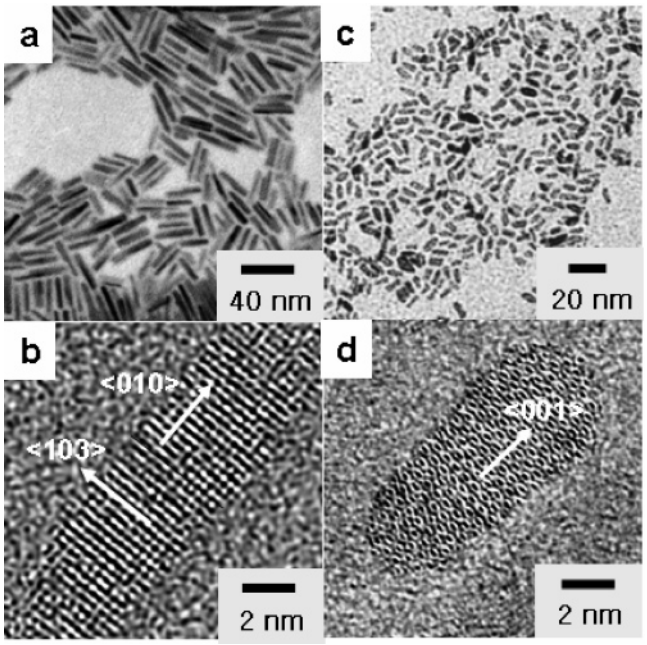

Figure 11. TEM and HR-TEM images of anisotropically grown $W_{18}O_{49}$ and Mn_3O_4 nanorods: (a, b) $W_{18}O_{49}$, (c, d) Mn_3O_4.

directions, since the growth rate is exponentially proportional to the surface energy. The growth rate along the ⟨001⟩ directions is much faster compared to other directions, which finally results in progressive elongation along the ⟨001⟩ directions of the nanocrystals and formation of one-dimensional rod structures (Figure 10).

Similar growth patterns are observed in the $W_{18}O_{49}$, Mn_3O_4, and TiO_2 nanocrystal growth.[39] The $W_{18}O_{49}$ has a monoclinic structure with a highly anisotropic *b*-axis (the *b*-axis being 0.2 times the *a*- and *c*-axes) with the highest atom packing density of {010} faces. The Mn_3O_4 and the TiO_2 both have tetragonal structures with anisotropic *c*-axes (*c*-axis/*a*-axis ratio: ∼1.7 (Mn_3O_4), ∼2.7 (TiO_2)) and the {001} faces have the highest packing density. As expected by the surface energy trend, the $W_{18}O_{49}$ nanorods elongated along the [010] direction are formed by thermal reactions of tungsten chloride with capping molecule mixtures containing oleic acid and oleylamine (Figure 11a,b), while Mn_3O_4 (Figure 11c,d) and TiO_2 (Figure 12) rods, synthesized using $MnCl_2$ and $TiCl_2$ respectively, are formed by the unidirectional growth along the [001] direction.

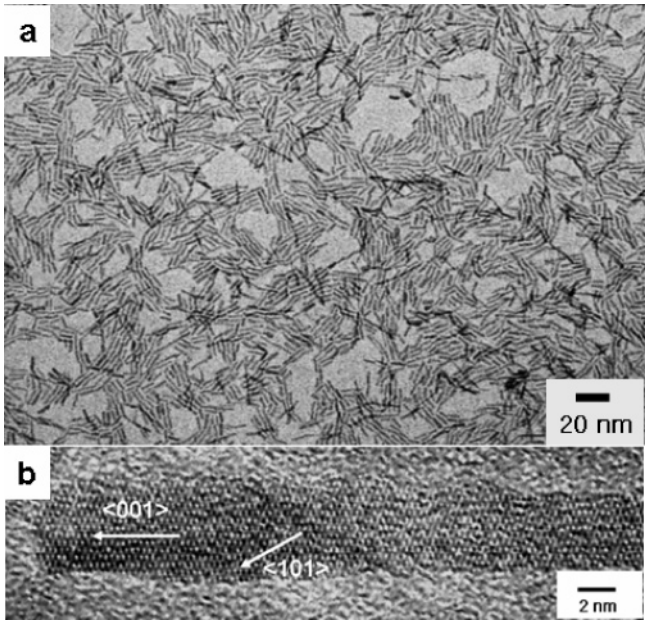

Figure 12. (a) TEM and (b) HR-TEM images of TiO_2 nanorods.

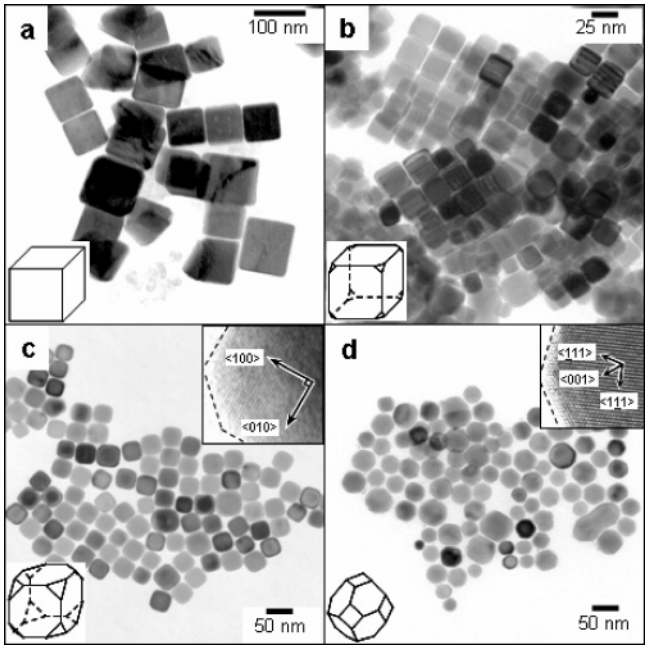

Figure 13. PbS nanocrystals. (a) cubes, (b, c) truncated cubes, (d) tetradecahedrons.

The surface energy dependent shape control of nanocrystals can be elaborated by modulating the relative surface energies with the use of surface selective capping molecules. Rock-salt phase PbS crystals generally nucleate as tetradecahedron seeds, exposing six {100} faces and eight {111} faces.[31] Since the intrinsic surface energy of the {111} faces is higher than that of the {100} faces, relatively fast growth along the eight equivalent ⟨111⟩ directions from the tetradecahedron seeds results in the formation of cube-shaped nanocrystals. When the nanocrystals are synthesized through the thermal decomposition of molecular precursors $Pb(S_2CNEt_2)_2$ in a hot organic solution containing dodecylamine as nonselective capping molecules, cube-shaped PbS nanocrystals are obtained (Figure 13a). The use of dodecanethiol as capping molecules instead of dodecylamine allows the systematic shape evolution of PbS nanocrystals. The dodecanethiol molecules tend to selectively stabilize the {111} faces via μ^3-Pb_3−SR bridging bonds, while they weakly bind to the {100} faces via a single bonding mode (Figure 14).[58] Therefore, the surface energy of the {111} faces can selectively be lowered relative to that of the {100} faces. The cube shapes of PbS nanocrystals are gradually changed to truncated octahedrons via truncated cubes, as the dodecanethiol concentration is increased. (Figure 13, b−d) The increase in R factor (r_{100}/r_{111}, the ratio of the central distance of the {100} faces to that of the {111} faces) from 0.60 to 0.79 and 0.98 by increasing dodecanethiol concentration also reveals that the higher concentration of dodecanthiol blocks the growth on the {111} faces and facilitates the growth on the {100} faces.

The one-dimensional shape evolution of TiO_2 anatase nanocrystals can also be a good example for examining the surface energy effect (Figure 15).[38] TiO_2 anatase has a tetragonal structure and has been shown to nucleate as truncated octagonal bipyramid seeds, exposing eight equivalent {101} faces and two equivalent {001} faces.[59] According to Donay-Harker rules, the surface energy of the {001} faces is ∼1.4 times larger than that for the {101} faces.[60] The significant difference of the intrinsic

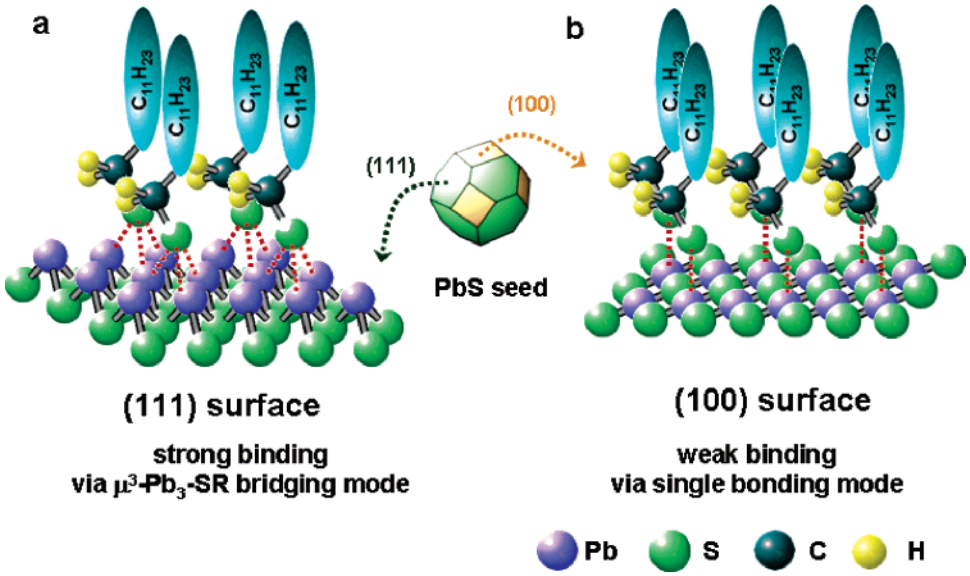

Figure 14. Binding modes of alkylthiols on PbS crystals: (a) μ^3-Pb_3−SR bridging mode on {111} surfaces, (b) single bonding mode on {100} surfaces.

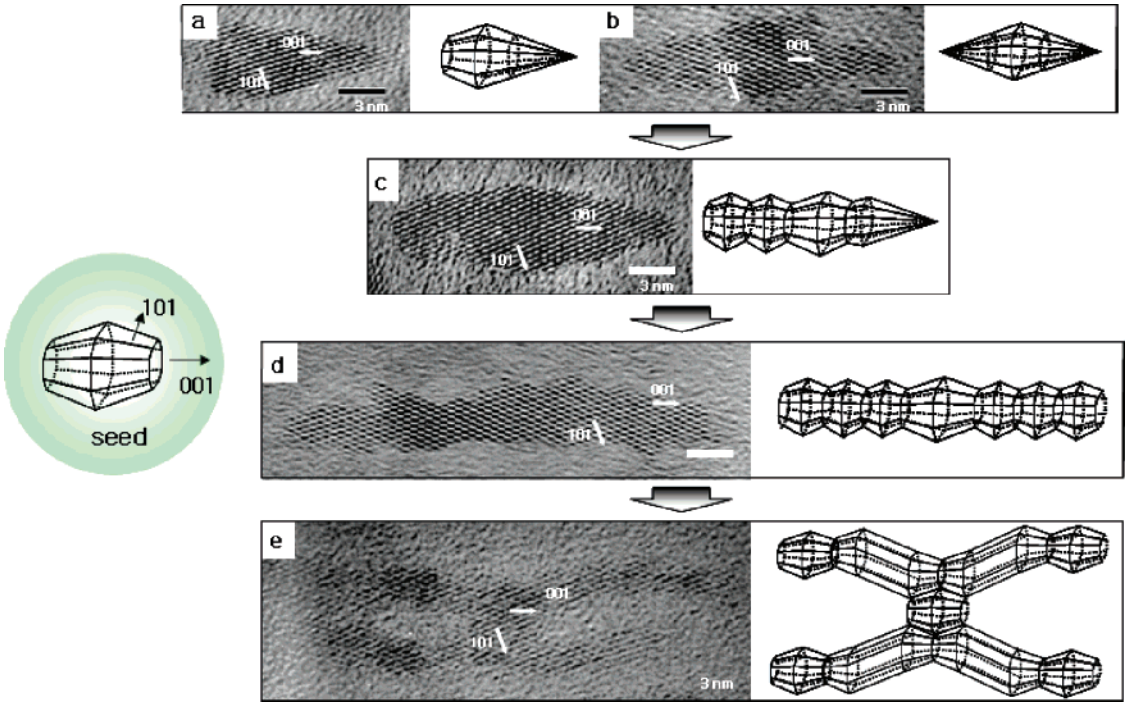

Figure 15. Shape evolution of TiO_2 nanocrystals depending on the concentration of lauric acid molecules: (a) bullets, (b) diamonds, (c) short rods, (d) long rods, (e) branched rods.

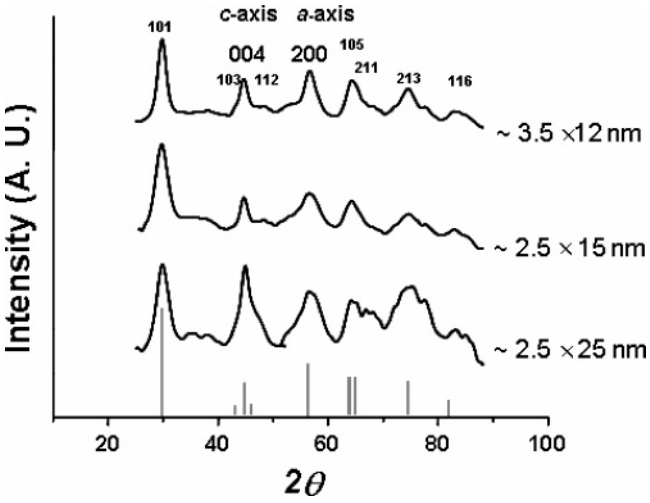

Figure 16. Anisotropic effect of TiO_2 nanocrystals on XRD patterns.

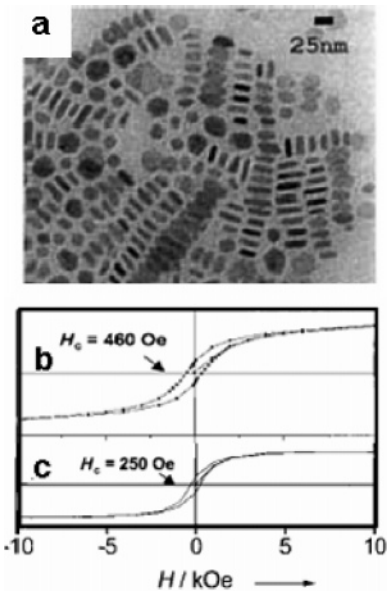

Figure 17. Co nanodisks: (a) TEM image, (b,c) magnetic coercivities of (b) disks (4 × 20 nm) and (c) spheres (13 nm).

surface energy induces the formation of bullet- and diamond-shaped nanocrystals, arising from the shrinking of the {001} faces and the complete elimination of the {001} faces at one or two ends of the truncated octahedral bipyramid seed, respectively (Figure 15a,b). However, when organic acid molecules are involved as capping molecules in the reaction, the capping molecules selectively bind to the {001} faces and reduce the growth rate along the ⟨001⟩ directions.[61] Under the reduced growth rate along the [001] direction, which is close to 2.7 times that of the [101] direction, monomers continuously grow further onto both the {001} and the {101} faces of the truncated octahedral bipyramid seeds. This results in the progressive elongation along the [001] direction while the [001] surface area is preserved (Figure 15c,d). Further retardation of the growth rate along the [001] direction, at a higher concentration of organic acid, induces the formation of branched nanorods, which is a result of the growth from the equivalent {101} faces of the truncated octahedral bipyramid seeds (Figure 15e). The surface energy modulation effects on the TiO_2 nanocrystal growth patterns are further confirmed from the observation of characteristic X-ray diffraction patterns of the anisotropic nanocrystals (Figure 16). A gradual increase in the relative (004)/(200) intensities and a sharpening of the (004) peak is observed in the spectra as the nanocrystal shape evolves bullets and diamonds to short rods and long rods as a consequence of the extended crystalline domain along the *c*-axis.

Two-dimensional growth of nanocrytals also can be achieved through controlling the crystallographic surface energies. Hexagonally close packed Co crystals have intrinsically higher energy surfaces of {001} compared to other crystallographic surfaces such as {100} and {110}. Therefore, one-dimensional growth of Co nanocrystals along the *c*-axis is expected. However, in the presence of alkylamine-capping molecules, Co nanocrystals are obtained as disk shapes compressed along the

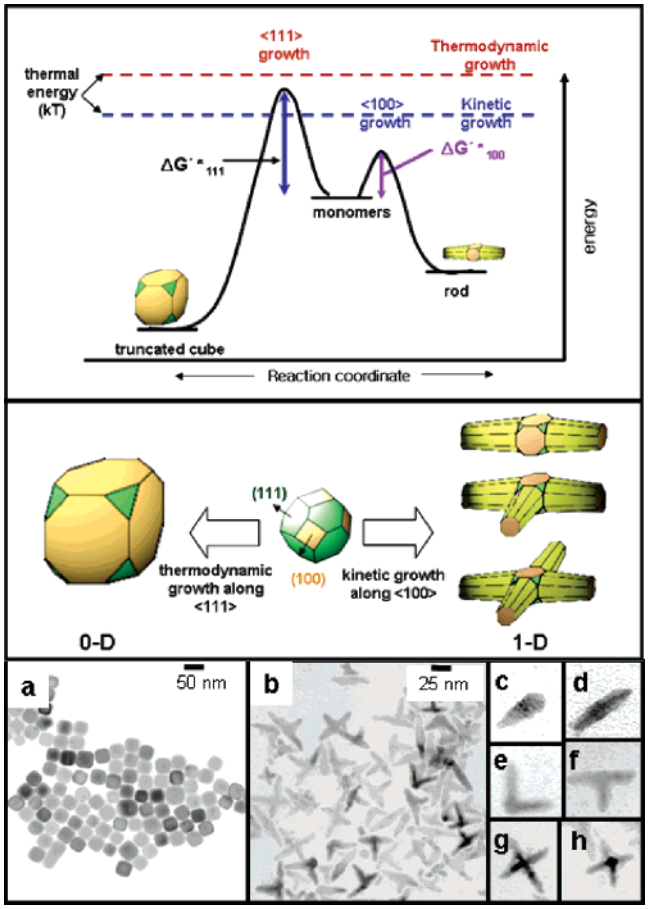

Figure 18. Growth regime dependent PbS nanocrystal shape control: (a) thermodynamically induced truncated cube shapes of PbS, (b−h) kinetically induced mono- and multipods of PbS.

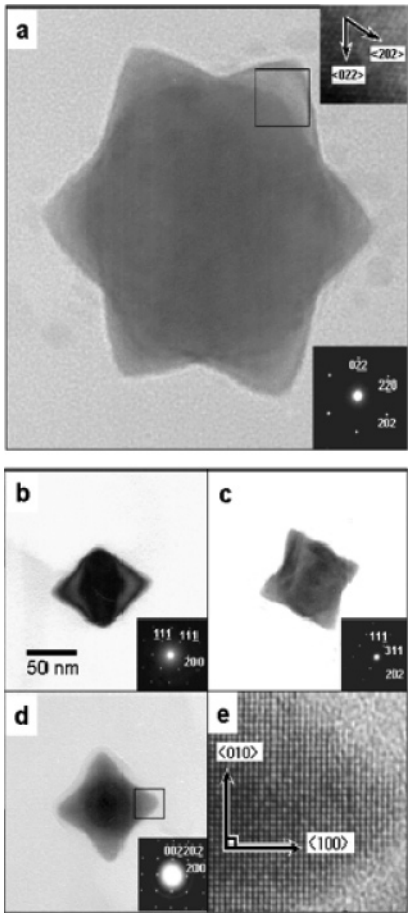

Figure 19. Star-shaped PbS nanocrystals. (a) TEM image of star-shaped PbS nanocrystals synthesized at 230 °C. (Inset) HR-TEM image of lattice fringes with zone axis of [111]. (b−d) TEM images and electron diffraction patterns with zone axis of (b) [110], (c) [112], (d) [100], respectively. (e) HR-TEM image of zoomed fringes with zone axis of [100].

c-axis rather than as rod shapes (Figure 17a).[47] This can be understood by the role of surface selective alkylamine capping molecules.[46,47] The surface energy of {001} can be selectively lowered through strong binding of alkylamines onto the {001} surfaces, and therefore growth along the ⟨001⟩ directions is inhibited. This induces relatively faster growth along the ⟨100⟩ and ⟨110⟩ directions, compared to the growth along the ⟨001⟩ directions, which finally results in the formation of disk shapes of Co nanocrystals. The anisotropic shape of Co nanodisks strongly influences their magnetic property. In the magnetic hysteresis loop of Co nanocrystals at 5 K presented in Figure 17b,c, the magnetic coercivity of Co nanodisks of 4 nm in height and 20 nm in diameter has a higher value of 460 Oe when compared to that of 13 nm spheres (250 Oe). Considering that the number of magnetic spins of the nanodisks is very close to that of the spheres, these shape-dependent unique magnetic phenomena are due to the increased magnetic anisotropies arising from the disk shape.[47]

c. Control of the Growth Regime: Kinetic vs Thermodynamic. Another critical growth parameter for shape determination is the delicate balance between the kinetic and the thermodynamic growth regimes. Under the thermodynamic growth regime that is characterized by a sufficient supply of thermal energy (*kT*) and low flux of monomer, monomers grow isotropically from the nucleating seeds, and therefore the formation of zero-dimensional structures (e.g., spheres) is preferred. Spheres are the thermodynamically most stable shape with the lowest overall surface energy. In contrast, under the nonequilibrium kinetic growth regime with a high flux of monomers, preferential anisotropic growth is facilitated along the kinetically most favorable direction with low activation energy barriers.

The control of growth regime between kinetic vs thermodynamic growth can be achieved by changing the reaction parameters such as the monomer concentration and the growth temperature.[23,24,31,34] The monomer concentration effects on the shape evolution of CdSe nanocrystals were extensively studied by Peng and co-workers.[24] At a low concentration of monomers at a fixed growth temperature, thermodynamically favorable, isotropic growth from the wurtzite seeds is preferred, which results in the formation of nanospheres. However, at a higher monomer concentration, kinetically favorable, anisotropic growth along the [00$\underline{1}$] direction of the wurtzite CdSe is favored, since the difference in growth rate between the [00$\underline{1}$] direction and other directions is accentuated by increasing the monomer concentration.

The shape evolution of rock-salt phased PbS nanocrystals provides a good example of the growth temperature effects on the choice of growth regime.[31] As described, PbS nucleates as tetradecahedron truncated with eight {111} faces and six {100} faces. When excess thermal energy is supplied at high growth temperature (∼300 °C), the thermodynamic regime governs the major growth process. In this growth regime, nearly isotropic growth from the tetradecahedron seeds is favored, and therefore cube shapes of PbS are obtained (Figure 18a). However, under the conditions of low temperature (∼140 °C) and in the presence of surface selective dodecanethiol molecules, the growth process

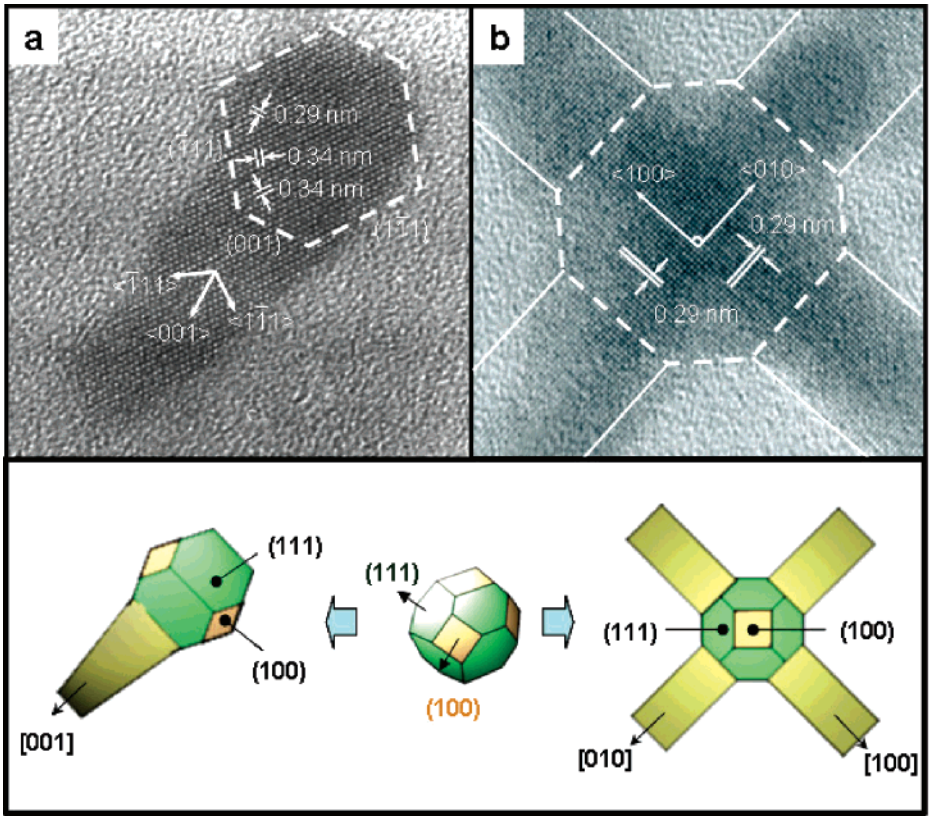

Figure 20. HR-TEM images of PbS nanocrystals grown at 140 °C: (a) tadpole-shaped, (b) cross-shaped nanocrystals.

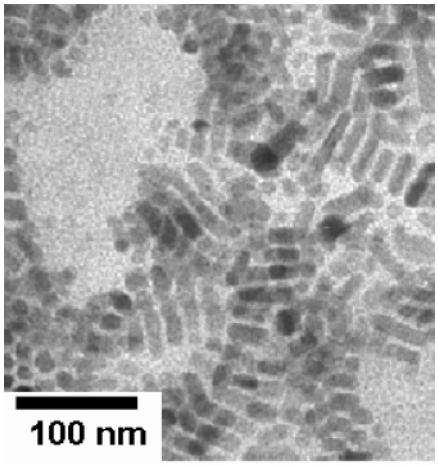

Figure 21. TEM images of $Cd_{0.88}Mn_{0.12}S$ nanorods.

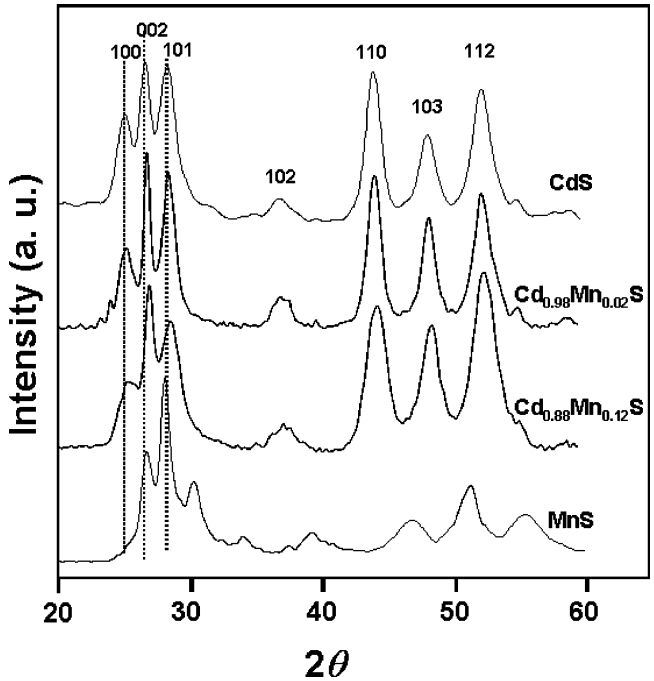

Figure 22. Dopant-level dependent XRD spectra of $Cd_{1-x}Mn_xS$ nanocrystals.

shifts into the kinetic growth regime and anisotropic growth on the {100} faces with high surface energy from the tetradecahedron seed is preferred. Remember that {111} faces are selectively stabilized under the presence of dodecanethiol molecule (see section IIIb). This results in one-dimensional rod-based multipod structures (Figure 18b−h). Interestingly, star-shaped nanocrystals, as a transient species between isotropic zero-dimensional and anisotropic one-dimensional shapes, are obtained at an intermediate growth temperature (∼180 °C) (Figure 19). TEM and electron diffraction (ED) analyses, by tilting the star-shaped nanocrystals with different zone axes, reveal that the nanocrystals resulted from the fast growth and progressive shrinking of the {100} faces into sharp triangular corners.

Crystal structures and growth patterns of these various nanoarchitectures of PbS examined by HR-TEM analyses support such growth processes. As shown in Figure 18a, the octagonal shape with four {111} and four {100} faces is observed from PbS nanocrystals synthesized at 300 °C, which is a two-dimensional projection of truncated cubes along the [100] direction. In contrast, the HR-TEM image of tadpole-shaped nanocrystals prepared at 140 °C and the interplanar distance measurements indicate that the rod grows along the [001] direction from the hexagonal shape (i.e., the [110] projection of tetradecahedron seed) (Figure 20a). Similarly, cross-shaped nanocrystals elongated along four [100] directions

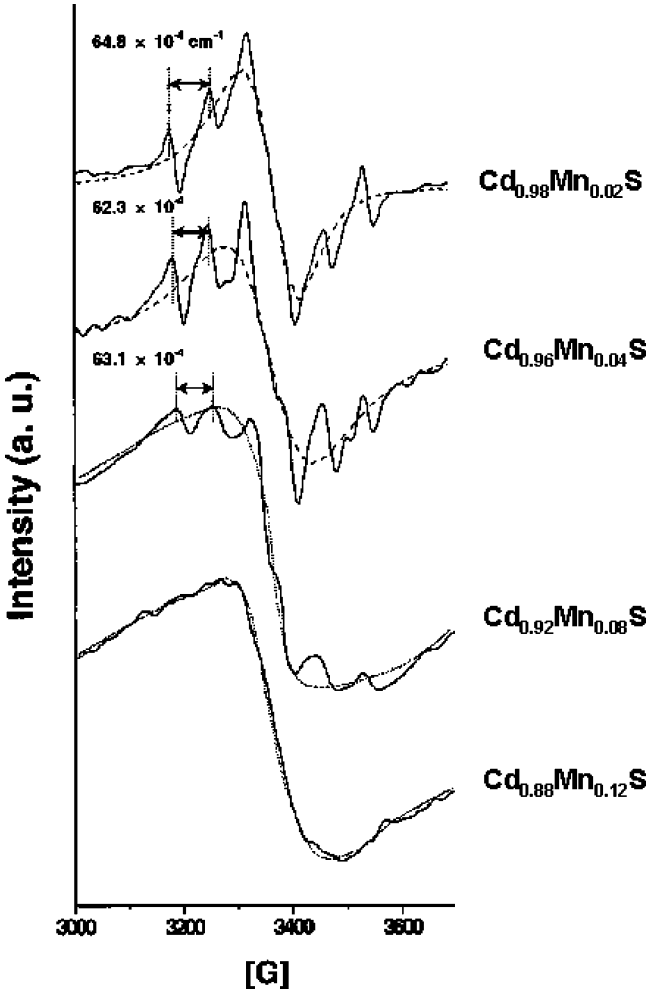

Figure 23. Electron paramagnetic resonance (EPR) analyses of $Cd_{1-x}Mn_xS$ nanocrystals.

from the octagonal shape (i.e., [100] projection of tetradecahedron seed) are also observed (Figure 20b).

The balance between these two growth regimes also enables the composition control of nanocrystals as well as the anisotropic shape control. One of the interesting systems for such composition and shape controlled growth is the anisotropic $Cd_{1-x}Mn_xS$ ($0.02 \leq x \leq 0.12$) diluted magnetic semiconductor nanocrystals.[34] The use of both the magnetic spin and the electron charge of diluted magnetic semiconductors makes the development of a synchronized system of the information processing and storage possible.[62−64] Until now, the formation of colloidal nanocrystals with a homogeneous distribution at high dopant levels has been difficult because of the easy segregation of Mn dopants from the host matrix under the high temperature thermodynamically driven synthetic conditions.[65,66] However, low-temperature kinetic growth strategy allows not only the homogeneous doping of Mn atoms with high doping levels (up to ~12%) but also the one-dimensional growth monorod formation, when $Cd(S_2CNEt_2)$ and $Mn(S_2CNEt_2)$ precursor molecules are co-injected into the hot alkylamine capping molecule solution. TEM (Figure 21), XRD (Figure 22), and electron paramagnetic resonance (EPR) analyses (Figure 23) clearly confirm the formation of one-dimensional $Cd_{1-x}Mn_xS$ ($0.02 \leq x \leq 0.12$) diluted magnetic semiconductor nanocrystals with homogeneous distribution of Mn atoms inside the CdS matrix. These results indicate that successful shape and composition control of nanocrystals is possible by the control of the growth regimes.

IV. Concluding Remarks and Future Directions

Nanoscale controllability of inorganic crystals can be achieved by a systematic understanding of their growth processes and of key factors related to the nanocrystal growth processes. In particular, we have discussed the important shape-guiding parameters and their roles on the shape determination. The crystalline phase of nucleation seeds, the surface energy, and the choice of crystal growth regimes are found to be crucial. These parameters can be modulated by controlling reaction conditions such as growth temperature, the use of surface selective capping molecules, and monomer concentration. Control of these key parameters has yielded a variety of inorganic nanocrystal shapes with multiple dimensionalities.

In addition to those nanocrystals investigated in this feature article, various synthetic methods have now been reported for structurally novel nanocrystals. Even for such successes as ours and others,[67−75] the syntheses have been mostly limited to zero- and one-dimensional shapes of nanocrystals and a narrow range of materials systems. Further development and extension of current synthetic strategies should be performed on a variety of materials and shapes, especially more advanced nanocrystal structures. One such advanced nanocrystal system can be a multicomponent nanostructure designed for unique functionality. The success of this field depends heavily on the development of more versatile but reliable synthetic schemes for the tailored nanocrystalline architectures of nanocrystals with desired components. Many new and as of yet undiscovered nanocrystals will become the key components for further scientific and technological applications. Therefore, the systematic elucidation of nanoscale physical properties of novel nanocrystals should accompany their synthetic protocols, with aspects of both theoretical and experimental approaches.

Acknowledgment. We thank KBSI for High Voltage Electron Microscopic (HVEM) and TEM analyses. This work is supported by the Korea Research Foundation (KRF-2004-041-C00186).

References and Notes

(1) Alivisatos, A. P. *Science* **1996**, *271*, 933.
(2) Brus, L. E. *J. Chem. Phys.* **1984**, *80*, 4403.
(3) Markovich, G.; Collier, C. P.; Henrichs, S. E.; Remacle, F.; Levine, R. D.; Heath, J. R. *Acc. Chem. Res.* **1999**, *32*, 415.
(4) Hu, J.; Odom, T. W.; Lieber, C. M. Acc. *Chem. Res.* **1999**, *32*, 435.
(5) Yang, P. *MRS Bull.* **2005**, *30*, 85.
(6) Law, M.; Goldberger, J.; Yang, P. *Annu. Rev. Mater. Res.* **2004**, *34*, 83.
(7) Bakkers, E. P. A. M.; Verheijen, M. A. *J. Am. Chem. Soc.* **2003**, *125*, 3440.
(8) Goldberger, J.; He, R. R.; Zhang, Y. F.; Lee, S. W.; Yan, H. Q.; Choi, H. J.; Yang, P. D. *Nature* **2003**, *422*, 599.
(9) Pan, Z. W.; Dai, Z. R.; Wang, Z. L. *Science* **2001**, *291*, 1947.
(10) Kong, X. Y.; Ding, Y.; Yang, R. S.; Wang, Z. L. *Science* **2004**, *303*, 1348.
(11) Saito, Y.; Matsumoto, T. *Nature* **1998**, *392*, 237.
(12) Gao, P. X.; Wang, Z. L. *J. Phys. Chem. B* **2004**, *108*, 7534.
(13) Murray, C. B.; Norris, D. J.; Bawendi, M. G. *J. Am. Chem. Soc.* **1993**, *115*, 8706.
(14) Trentler, T. J.; Goel, S. C.; Hickman, K. M.; Viano, A. M.; Chiang, M. Y.; Beatty, A. M.; Gibbons, P. C.; Buhro, W. E. *J. Am. Chem. Soc.* **1997**, *119*, 2172.
(15) Trentler, T. J.; Hickman, K. M.; Goel, S. C.; Viano, A. M.; Gibbons, P. C.; Buhro, W. E. *Science* **1995**, *270*, 1791.
(16) Holmes, J. D.; Johnston, K. P.; Doty, R. C.; Korgel, B. A. *Science* **2000**, *287*, 1471.
(17) Shah, P. S.; Hanrath, T.; Johnston, K. P.; Korgel, B. A. *J. Phys. Chem. B* **2004**, *108*, 9754.
(18) Kan, S.; Mokari, T.; Rothenberg, E.; Banin, U. *Nature Mater.* **2003**, *2*, 155.

(19) Peng, X.; Manna, L.; Yang, W.; Wickham, J.; Scher, E. C.; Kadavanich, A.; Alivisatos, A. P. *Nature* **2000**, *404*, 59.
(20) Peng, Z. A.; Peng, X. *J. Am. Chem. Soc.* **2002**, *124*, 3343.
(21) Joo, J.; Na, H. B.; Yu, T.; Yu, J. H.; Kim, Y. W.; Wu, F.; Zhang, J. Z.; Hyeon, T. *J. Am. Chem. Soc.* **2003**, *125*, 11100.
(22) Jun, Y.; Lee, S.-M.; Kang, N.-J.; Cheon, J. *J. Am. Chem. Soc.* **2001**, *123*, 615.
(23) Manna, L.; Scher, E. C.; Alivisatos, A. P. *J. Am. Chem. Soc.* **2000**, *122*, 12700.
(24) Peng, Z. A.; Peng, X. *J. Am. Chem. Soc.* **2001**, *123*, 1389.
(25) Manna, L.; Million, D. J.; Miesel, A.; Scher, E. C.; Alivisatos, A. P. *Nature Mater.* **2003**, *2*, 382.
(26) Tang, Z.; Kotov, N. A.; Giersig, M. *Science* **2002**, *297*, 237.
(27) Cozzoli, P. D.; Manna, L.; Curri, M. L.; Kudera, S.; Giannini, C.; Striccoli, M.; Agostiano, A. *Chem. Mater.* **2005**, *17*, 1296.
(28) Kim, Y.-H.; Jun, Y.; Jun, B.-H.; Lee, S.-M.; Cheon, J. *J. Am. Chem. Soc.* **2002**, *124*, 13656.
(29) Ahrenkiel, S. P.; Micic, O. I.; Miedaner, A.; Curtis, C. J.; Nedeljkoic, J. M.; Nozik, A. J. *Nano Lett.* **2003**, *3*, 833.
(30) Gerion, D.; Zitseva, N.; Saw, C.; Casula, M. F.; Fakra, S.; Buuren, T. V.; Galli, G. *Nano Lett.* **2004**, *4*, 597.
(31) Lee, S.-M.; Jun, Y.; Cho, S.-N.; Cheon, J. *J. Am. Chem. Soc.* **2002**, *124*, 11244.
(32) Lifshitz, E.; Bashout, M.; Kigel, A.; Eisen, M. S.; Berger, S. *Nano Lett.* **2003**, *3*, 857.
(33) Cho, K.-S.; Talapin, D. V.; Gaschler, W.; Murray, C. B. *J. Am. Chem. Soc.*, in press.
(34) Jun, Y.; Jung, Y.; Cheon, J. *J. Am. Chem. Soc.* **2002**, *124*, 615.
(35) Yin, M.; Gu, Y.; Kuskovsky, I. L.; Andelman, T.; Zhu, Y.; Neumark, G. F.; O'Brien, S. *J. Am. Chem. Soc.* **2004**, *126*, 6206.
(36) Mouge, M.; Kahn, M. L.; Maisonnat, A.; Chaudret, B. *Angew. Chem., Int. Ed.* **2003**, *42*, 5321.
(37) Niederberger, M.; Bartl, M.-H.; Stucky, G. D. *J. Am. Chem. Soc.* **2002**, *124*, 13642.
(38) Jun, Y.; Casula, M. F.; Sim, J.-H.; Kim, S. Y.; Cheon, J.; Alivisatos, A. P. *J. Am. Chem. Soc.* **2003**, *125*, 15981.
(39) Seo, J.; Jun, Y.; Ko, S. J.; Cheon, J. *J. Phys. Chem. B* **2005**, *109*, 5389.
(40) Lee, K.; Seo, W. S.; Park, J. T. *J. Am. Chem. Soc.* **2003**, *125*, 3408.
(41) Park, J.; Kang, E.; Bae, C. J.; Park, J.-G.; Noh, H.-J.; Kim, J.-Y.; Park, J.-H.; Park, H.-M.; Hyeon, T. *J. Phys. Chem. B* **2004**, *108*, 13594.
(42) Urban, J. J.; Yun, W. S.; Gu, Q.; Park, H. *J. Am. Chem. Soc.* **2002**, *124*, 1186.
(43) Cheon, J.; Kang, N.-J.; Lee, S.-M.; Lee, J.-H.; Yoon, J.-H.; Oh, S.-J. *J. Am. Chem. Soc.* **2004**, *126*, 1950.
(44) Larsen, T.-H.; Sigman, M.; Ghezelbash, A.; Doty, R. C.; Korgel, B. A. *J. Am. Chem. Soc.* **2003**, *125*, 5638.
(45) Ghezelbash, A.; Sigman, M.; Doty, R. C.; Korgel, B. A. *Nano Lett.* **2004**, *4*, 537.
(46) Puntes, V. F.; Zanchet, D.; Erdonmez, C. K.; Alivisatos, A. P. *J. Am. Chem. Soc.* **2002**, *124*, 12874.
(47) Park, J.-I.; Kang, N.-J.; Jun, Y.; Oh, S.-J.; Ri, H. C.; Cheon, J. *ChemPhysChem* **2002**, *3*, 543.
(48) Cordente, N.; Respauel, M.; Senocq, F.; Casanova, M.-J.; Amiens, C.; Chaudret, B. *Nano Lett.* **2001**, *1*, 565.
(49) Dumestre, F.; Chaudret, B.; Amiens, C.; Respaud, M.; Fejes, P.; Renaud, P.; Zurcher, P. *Angew. Chem. Int. Ed.* **2003**, *42*, 5213.
(50) Teng, X.; Yang, H. *Nano Lett.* **2005**, *5*, 885.
(51) Cao, Y. C. *J. Am. Chem. Soc.* **2004**, *126*, 7456.
(52) *Dictionary of Inorganic Compounds*, 1st ed.; Macintyre, J. E., Ed.; Chapman & Hall: London, New York, 1992.
(53) Lu, J.; Qi, P.; Peng, Y.; Meng, Z.; Yang, Z.; Yu, W.; Qian, Y. *Chem. Mater.* **2001**, *13*, 2169.
(54) Zelaya-Angel, O.; Alvaradi-Gol, J. J.; Lozada-Morales, R.; Vargas, H.; Ferreira da Silva, A. *Appl. Phys. Lett.* **1994**, *64*, 291.
(55) Yeh, C.-Y.; Lu, Z. W.; Froyen, S.; Zunger, A. *Phys. Rev. B* **1992**, *46*, 10086.
(56) Micic, O. I.; Sprague, J. R.; Curtis, C. J.; Jones, K. M.; Machol, J. L.; Nozik, A. J.; Giessen, H.; Fluegel, B.; Mohs, G.; Peyghambarian, N. *J. Phys. Chem.* **1995**, *99*, 7754.
(57) Hu, J.; Li, L.-S.; Yang, W.; Manna, L. Wang, L. *Science* **2001**, *292*, 2060.
(58) Sugimoto, T. *J. Phys. Chem. B* **2000**, *104*, 1153.
(59) Penn, R. L.; Banfield, J. F. *Geochim. Cosmichim. Acta* **1999**, *63*, 1549.
(60) Donnay, J. D.; Harker, D. *Am. Mineral.* **1937**, *22*, 446.
(61) Tanner, R. E.; Liang, Y.; Altman, E. I. *Surf. Sci.* **2002**, *506*, 251.
(62) Ohno, H. *Science* **1998**, *281*, 951.
(63) Dietl, T.; Ohno, H.; Matsukura, F.; Clibert, J.; Ferrand, D. *Science* **2000**, *287*, 1019.
(64) Awschalom, D. D.; Kawakami, R. K. *Nature* **2000**, *408*, 923.
(65) Mikulec, F. V.; Kuno, M.; Bennati, M.; Hall, D. A.; Griffin, R. G.; Bawendi, M. G. *J. Am. Chem. Soc.* **2000**, *122*, 2532.
(66) Norris, D. J.; Yao, N.; Charnock, F. T.; Kennedy, T. A. *Nano Lett.* **2001**, *1*, 3.
(67) Sun, S.; Murray, C. B.; Weller, D.; Folks, L.; Moser, A. *Science* **2000**, *287*, 1989.
(68) Park, J.-I.; Cheon, J. *J. Am. Chem. Soc.* **2001**, 123, 5743.
(69) Mokari, T.; Rothenberg, E.; Popov, I.; Costi, R.; Banin, U. *Science* **2004**, *304*, 1787.
(70) Yu, H.; Chen, M.; Rice, P. M.; Wang, S. X.; White, R. L.; Sun, S. *Nano Lett.* **2005**, *5*, 379.
(71) Kudera, S.; Carbone, L.; Casula, M. F.; Cingolani, R.; Falqui, A.; Snoeck, E.; Parak, W. J.; Manna, L. *Nano Lett.* **2005**, *5*, 445.
(72) Kim, H.; Achermann, M.; Balet, L. P.; Hollingsworth, J. A.; Klimov, V. I. *J. Am. Chem. Soc.* **2005**, *127*, 544.
(73) Milliron, D. J.; Hughes, S. M.; Cui, Y.; Manna, L.; Li, J.; Wang, L.-W.; Alivisatos, A. P. *Nature* **2004**, *430*, 190.
(74) Zeng, H.; Li, J.; Liu, J. P.; Wang, Z. L.; Sun, S. *Nature* **2002**, *420*, 395.
(75) Redl, F. X.; Cho, K.-S.; Murray, C. B.; O'Brien, S. *Nature* **2003**, *423*, 968.